# Empirical Model for Electrical Activation of Aluminum- and Boron-Implanted Silicon Carbide

Vito Šimonka, Andreas Hössinger, Josef Weinbub, *Member, IEEE*, and Siegfried Selberherr, *Fellow, IEEE*

***Abstract*— Accurate modeling of the electrical properties of impurities in semiconductors is essential for the mandatory support of the development of novel semiconductor devices by means of simulations. An appropriate modeling approach to determine the activation rate of dopants in silicon carbide is currently not available, which limits the predictability of process simulations. To remedy this fact, we propose an empirical model for the electrical activation of aluminum and boron impurities in silicon carbide for various annealing temperatures and total doping concentrations. The differences of the two acceptor-type dopants are discussed according to the model predictions and the activation ratios for various processing parameters are presented. The model was implemented into Silvaco's simulation platform Victory Process and evaluated with respect to published experimental findings.**

***Index Terms*— Activation, aluminum, annealing, boron, implantation, modeling, silicon carbide, simulation.**

## I. Introduction

SILICON carbide (SiC) is a wide bandgap semiconductor with outstanding properties, such as high thermal conductivity, high electrical breakdown field, high temperature operation, and low reverse leakage current [1], [2]. Due to these attractive properties, SiC has been used in a series of promising applications for low-loss, high-power, and high-frequency electronic devices capable of operating in harsh environments [3]–[5]. However, despite of the advantageous properties, there are still many issues to be solved before the performance of SiC devices reaches its full potential [6]. One of the key factors of successful device fabrication is to accurately determine the electrical characteristics of impurities in SiC, which is an industrial and academic focus of recent years [7]–[11].

Manuscript received November 2, 2017; revised December 14, 2017 and December 19, 2017; accepted December 19, 2017. Date of publication January 4, 2018; date of current version January 22, 2018. This work was supported in part by the Austrian Federal Ministry of Science, Research and Economy and in part by the National Foundation for Research, Technology and Development. The review of this paper was arranged by Editor J. Mateos. *(Corresponding author: Vito Šimonka.)*

V. Šimonka and J. Weinbub are with the Christian Doppler Laboratory for High Performance TCAD, Institute for Microelectronics, TU Wien, 1040 Wien, Austria (e-mail: simonka@iue.tuwien.ac.at).

A. Hössinger is with Silvaco Europe Ltd., Cambridge PE27 5JL, U.K.

S. Selberherr is with the Institute for Microelectronics, TU Wien, 1040 Wien, Austria.

Color versions of one or more of the figures in this paper are available online at http://ieeexplore.ieee.org.

Digital Object Identifier 10.1109/TED.2017.2786086

A prevalent doping technique for SiC devices is ion implantation, which requires a mandatory post-implantation annealing step in order to recover the disorder in the semiconductor lattice produced by ion bombardment and to increase the electrical activation of the implanted impurities [9], [12]. Among the acceptor-type dopants in SiC, aluminum (Al) and boron (B) are most common, for which the effects of the post-implantation annealing are yet not fully understood [13]. One of the main issues with implantation in SiC is that the rate of the activation is decreased, i.e., saturated, at high doping levels [14]. Furthermore, the mechanisms of electrical activation of implanted impurities in SiC lack theoretical understanding. In particular, a computational modeling approach of the activation mechanism is completely missing, which therefore limits the capabilities of process simulations.

In this paper, we investigate the SiC post-implantation annealing and propose an empirical model for the electrical activation of the SiC dopants based on experimental data. We introduce temperature-dependent model parameters for Al and B impurities and perform numerous simulations to ensure consistency between experiments and theory.

## II. Method

The empirical model has been inherited and modified from the model for the electrical activation of dopants in silicon [15]. Our modification introduces a continuous transition between the linear and logarithmic component of the model, which enables model fitting on the whole scale of the investigated variables. The model is represented by the time-independent empirical formula and assumes that the activation mechanism is instantaneous. The acceptor concentration $N_A$ is thus described by

$$N_A = S_1 C_{\text{tot}} + S_2 C_{\text{th}} S_t \tag{1}$$

where

$$\begin{aligned} S_1 &= 1/2(1 + \tanh(C_{\text{th}} - C_{\text{tot}})) \\ S_2 &= 1/2(1 + \tanh(C_{\text{tot}} - C_{\text{th}})) \end{aligned} \tag{2}$$

and

$$S_t = \left(1 + (1 - F_{\text{act}}) \ln\left(\frac{|C_{\text{tot}}/C_{\text{th}} - F_{\text{act}}|}{1 - F_{\text{act}}}\right)\right). \tag{3}$$

$C_{\text{tot}}$ is the total concentration of dopants, $C_{\text{th}}$ is the dopant specific threshold concentration, $F_{\text{act}}$ is the empirical scalar

parameter, $S_t$ is the saturation ratio, and $S_1$ and $S_2$ are model prefactors.

For the total dopant concentration below the threshold concentrations ($C_{\text{tot}} < C_{\text{th}}$) the model suggests that after annealing at a given temperature the acceptor concentration equals the total doping concentration ($N_A = C_{\text{tot}}$). Note, $C_{\text{th}}$ varies with the annealing temperature, therefore, the regime of full dopant activation is indirectly temperature-dependent. For the total dopant concentration above the threshold concentration ($C_{\text{tot}} > C_{\text{th}}$) the model introduces dopant- and temperature-dependent saturation effects, described by (3). Thus, a continuous switching between the linear and the logarithmic region of the activation response is required, which is handled via prefactors (2) according to the difference between $C_{\text{tot}}$ and $N_A$. This is a key contribution of our modeling approach and enables model fitting and calibration of simulation tools.

Despite the complexity of the model expression, an advantage of the model is the low amount of free model parameters and its analytic nature; the computational complexity is thus significantly smaller than a microscopic simulation, e.g., a molecular dynamics simulation. In an industry-focused simulation context the empirical approach is thus preferred.

We have collected several sets of acceptor concentrations for Al- and B-implanted SiC for various implanted concentrations and annealing temperatures from [14] and [16]–[21]. For the references where the acceptor concentration is absent, the carrier concentrations as a function of the reciprocal temperature were collected. These plots were then fit with the charge neutrality equation [22] to obtain Al and B acceptor concentrations using the thermal ionization energy as a fitting parameter, shown in our previous study [23]. We have performed several iterations of least squares fitting method [24] to ensure minimal numerical error. The results of the neutrality equation fitting, i.e., acceptor concentrations, are shown in Fig. 1 as a function of the total concentration for various annealing temperatures. Note, the data in this representation is not available in the literature, but is a critical requirement for the model calibration, further underlining the importance of the conducted research.

Doping concentrations from $1\times10^{17}$ cm$^{-3}$ to $1\times10^{20}$ cm$^{-3}$ and annealing temperatures from 1300 °C to 1800 °C were investigated. We have considered only the data, which cover identical crystal orientations, annealing ambient, implantation temperatures, and measurement methods. This selection of the data is necessary to ensure a focused investigation of the annealing temperature. It is assumed that the different applied annealing methods (microwave, inductive, and resistive heating) result in equal activation ratios. However, all of the annealing steps are performed in argon ambience. We have focused our study on 4H- and 6H-SiC and did not assume any differences in activation rates between the hexagonal structures; the error due to this assumption is on average very small, i.e., <5% [17]. In addition, the fit data must satisfy the requirement of the model, i.e., the activation state at the thermodynamic equilibrium. Although, these criteria limit the amount of relevant data for this paper, but in turn ensure a proper frame of reference for our model.

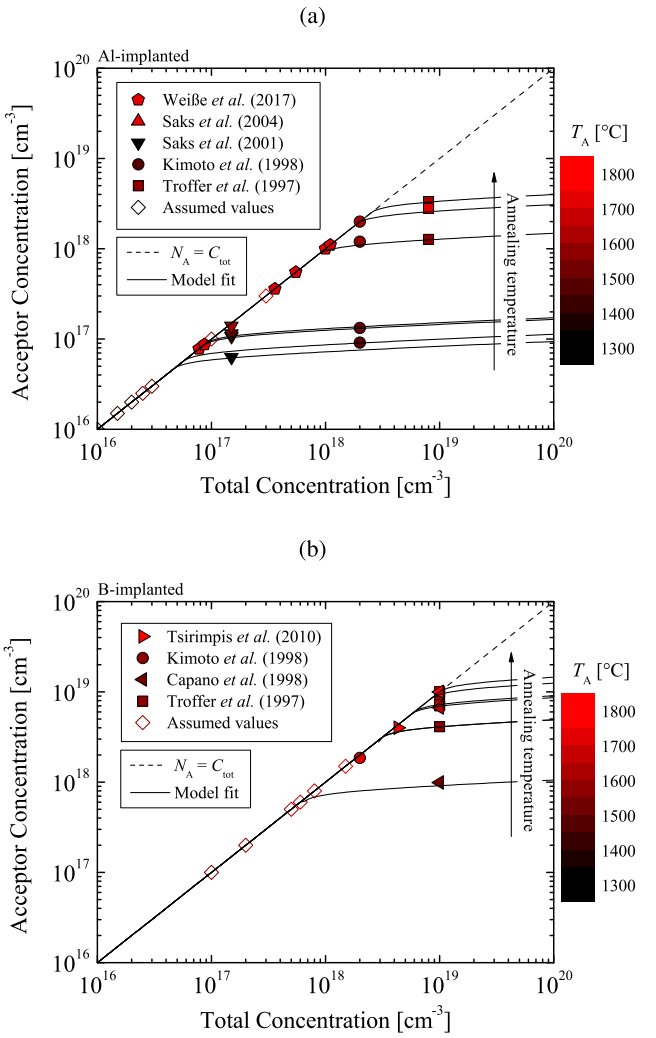


Fig. 1. Acceptor concentrations as a function of the total doping concentration for (a) Al- and (b) B-doped SiC. The closed symbols refer to [14] and [16]–[21] and the open symbols refer to the assumed values, which are used to increase the accuracy of the model fitting. The solid lines are model fits and the dashed lines indicate the linear dependence of $N_A$. Colors refer to the various annealing temperatures.

An iterative fitting method, evaluated by least squares error, was used to accurately fit the model (1-3) to the preprocessed data of the acceptor concentrations as a function of the total doping concentration. In order to minimize the numerical fitting error due to the low amount of relevant available data, we have assumed 100% activation for samples with low implanted concentration, which are annealed at high temperatures relative to the implanted dose. The model parameter $C_{\text{th}}$ for Al- and B-implanted SiC was obtained with respect to the various annealing temperatures. We have empirically determined that the best fits are accomplished for $F_{\text{act}} \approx 0.9$; therefore, from this point forward, the empirical scalar parameter is fixed to 0.9.

## III. Results and Discussion

The temperature-dependent parameter $C_{\text{th}}$ introduces the dopant concentration limit, where the saturation effects begin. The activation rate is significantly reduced (i.e., saturates) above the threshold for particular annealing temperature.

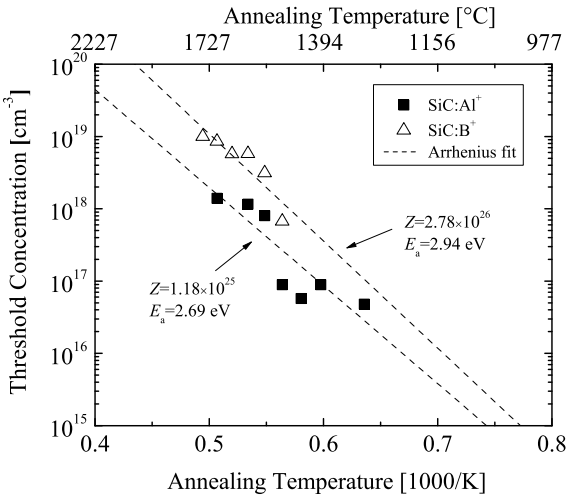


Fig. 2. Threshold concentration as a function of annealing temperature for Al- and B-doped SiC. The symbols refer to results obtained by the model fitting, and the dashed lines are Arrhenius fits.

We propose the threshold concentrations obtained by the model fitting for Al and B doped SiC, shown in Fig. 2. The threshold of B-doped SiC becomes significantly larger at high annealing temperatures than the threshold of Al-doped SiC. This effect is associated with the atomic mass of the dopants, i.e., B ions are lighter than Al ions [20]. An Arrhenius function was used in order to introduce a continuous temperature dependence of the model parameter. The best fit is achieved with the activation energy $E_a = 2.69$ eV and preexponential factor $Z = 1.18 \times 10^{25}$ cm$^{-3}$ for Al and $E_a = 2.94$ eV and $Z = 2.78 \times 10^{26}$ cm$^{-3}$ for B acceptors.

We have performed a parameter study based on $10^6$ simulations, to cover a wide range of parameter variations, of Al and B implantations followed by thermal annealing steps in order to characterize model predictions. The results of the simulations are shown in Fig. 3. The phase diagrams suggest activation regions of the dopants for various doping concentrations and annealing temperatures. These results are crucial to correctly predict parameters for SiC device processing, where the balance between the efficiency of electrical properties and the costs for post-implantation annealing must be carefully considered to optimize the fabrication processes. Cross sections of the phase diagrams are shown in Fig. 4 for various total concentrations. The simulations of annealing steps with a temperature below 1200 °C show relatively high activation for particular low-dose implantations. This suggests that process steps including temperatures above ≈600 °C, e.g., high temperature implantation, provide additional effects for electrical activation of impurities in SiC [14]. For the low-dose implantation ($C_{\text{tot}} = 1 \times 10^{15}$ cm$^{-3}$) the full activation state ($R_{\text{act}} = 1$) in a thermal equilibrium is achieved at $T_A = 1070$ °C for Al-implanted SiC and $T_A = 1010$ °C for B-implanted SiC. In contrast, for the high-dose implantation ($C_{\text{tot}} = 1 \times 10^{19}$ cm$^{-3}$), the full activation in thermal equilibrium is achieved at $T_A = 1940$ °C for Al-implanted SiC and $T_A = 1695$ °C for B-implanted SiC. In addition, for $C_{\text{tot}} = 1 \times 10^{20}$ cm$^{-3}$, the full activation of Al acceptors was not achieved even for the very high annealing temperatures

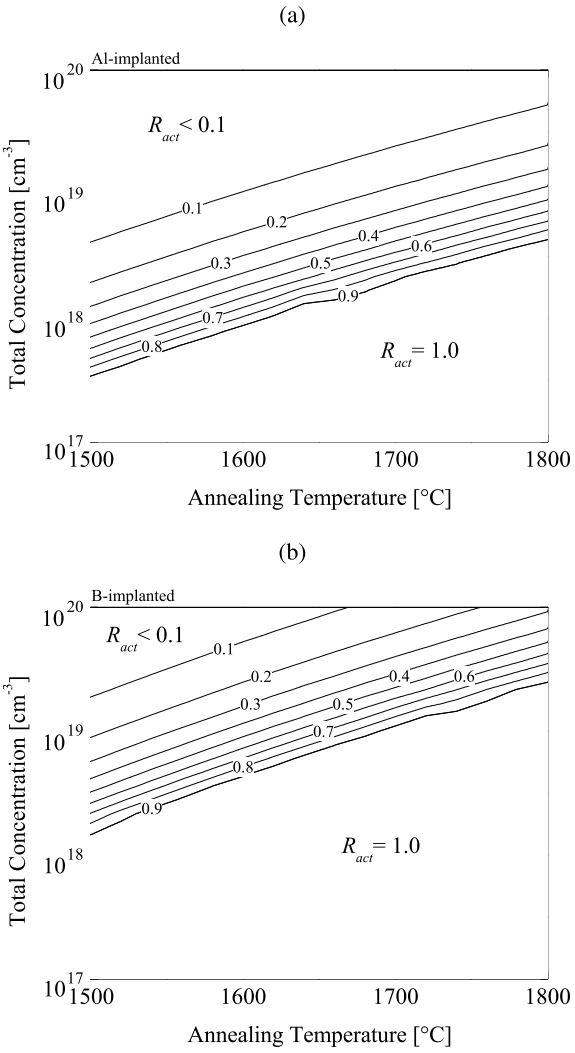


Fig. 3. Phase diagrams of predicted electrical activation ratios $R_{\text{act}}$ for (a) Al- and (b) B-doped SiC as a function of the total concentration and annealing temperature.

($T_A > 2200$ °C), but in contrast, B acceptors with the identical implantation dose reached full activation at $T_A = 2010$ °C.

The model was implemented into Silvaco's Victory Process simulator [15] together with the obtained model parameters. We have performed simulations of various annealing steps after Al and B implantations in SiC. The doping as well as the annealing steps follow the experimental setups of Saks *et al.* [17] and Troffer *et al.* [19] in order to enable an elaborate comparison. The implantation steps were performed with Silvaco's Victory Process simulator using Monte Carlo ion implantation on (0001) Si-oriented 4H-SiC. The annealing steps were performed with the proposed model and parameters, alongside with the Fermi diffusion model. An example of the simulated device is shown in Fig. 5. The simplicity of the simulated devices is vital in order to ensure the proper investigation of the process annealing steps only, including the total doping concentration and the annealing temperature.

The model was evaluated by strict comparisons between simulations and experiments, shown in Fig. 6. The first simulation setup [Fig. 6(a)] followed the experimental setup of Saks *et al.* [17], which consists of a nitrogen-doped, n-type SiC wafer with a compensation concentration of $\approx 5 \times 10^{15}$ cm$^{-3}$,

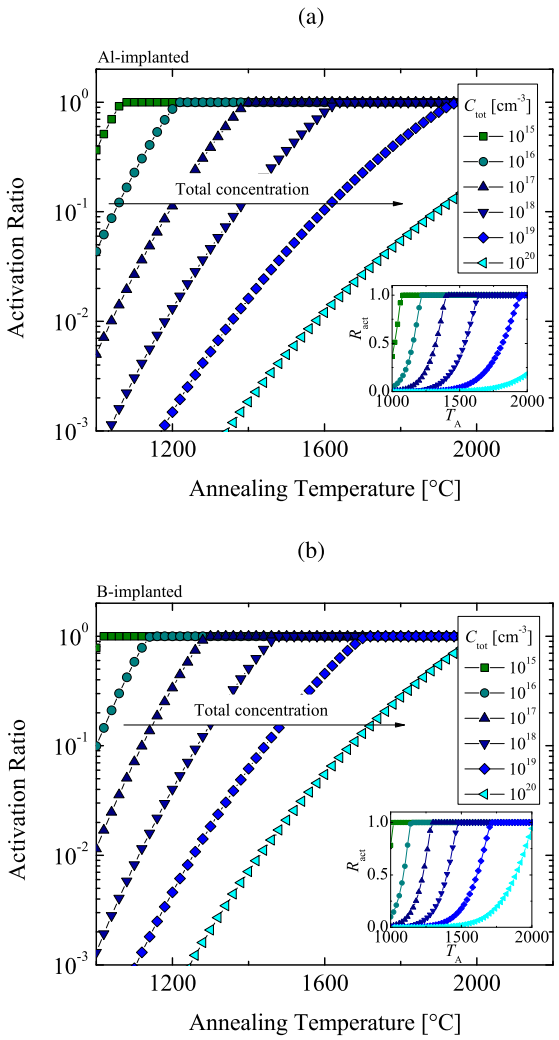


Fig. 4. Model predictions of activation ratio as a function of annealing temperature for (a) Al- and (b) B-doped SiC. Colors and symbols refer to various total doping concentrations $C_{tot}$ from $1 \times 10^{15}$ cm$^{-3}$ to $1 \times 10^{20}$ cm$^{-3}$. The inset figures use linear $y$-axes.

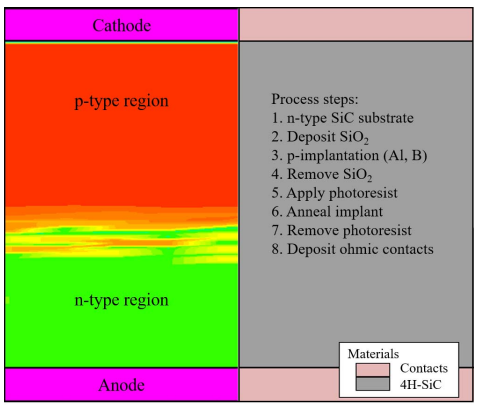


Fig. 5. Schematic representation of the doping profile and geometry of the processed device in the Victory Process simulator. The colors (left) refer to different doping regions, the gray region (right) is SiC substrate, and the light rose regions (right) are ohmic contacts, i.e., anode and cathode.

followed by several Al implantations generating a rectangular profile with a mean concentration of $\approx 1 \times 10^{17}$ cm$^{-3}$. The annealing steps were 12 hat $T_A = 1300$ °C, 1 hat

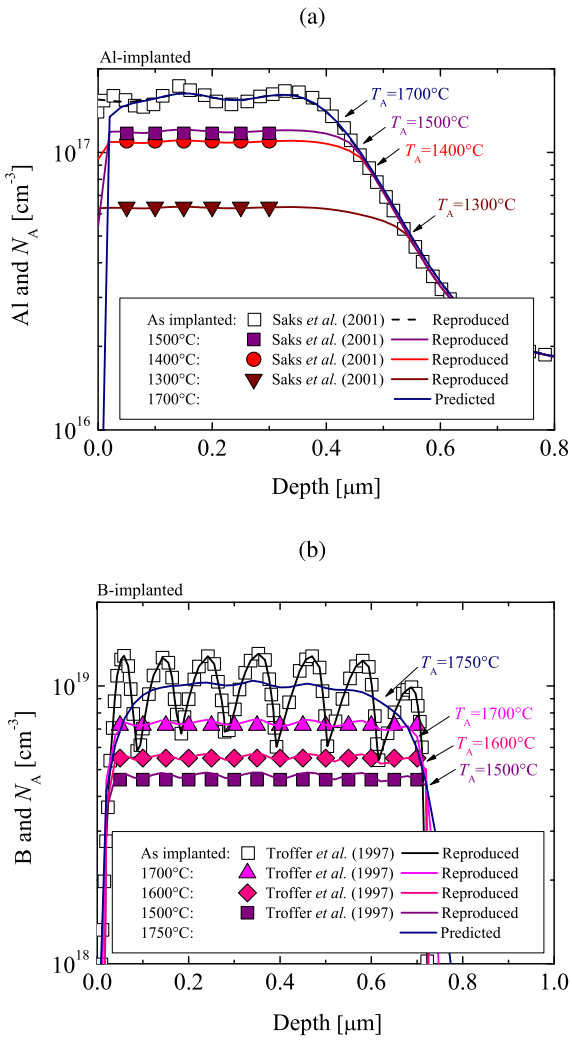


Fig. 6. Depth profiles of implanted dopant and annealed acceptor concentrations of (a) Al- and (b) B-doped SiC. Open symbols refer to the implanted profiles, colored symbols refer to the experimental data of average concentrations from Saks *et al.* [17] and Troffer *et al.* [19], and solid lines refer to the reproduced and predicted results obtained in this paper. The simulations were performed with the Victory Process simulator using Monte Carlo implantation, the Fermi diffusion model, and the activation model from this paper.

$T_A = 1400$ °C, and 10 min at $T_A = 1500$ °C. Note, the time of the thermal treatment influences the diffusion, but does not enter the proposed activation model. The second simulation setup [Fig. 6(b)] followed the experimental setup of Troffer *et al.* [19], which consists of a nitrogen-doped, n-type SiC wafer with a compensation concentration of $\approx 1.5 \times 10^{16}$ cm$^{-3}$, followed by several B implantations generating a rectangular profile with a mean concentration of $\approx 1 \times 10^{19}$ cm$^{-3}$. The annealing steps were 30 min at $T_A = 1500$ °C, 30 min at $T_A = 1600$ °C, and 30 min at $T_A = 1700$ °C.

The acceptor profiles were reproduced with an average variation $\sigma < 3\%$ for all of the annealing steps of both p-type dopants. The accurate reproduction of both implantation profiles and acceptor concentrations requires our modeling approach within the simulator to correctly predict the electrical characteristics of SiC devices.

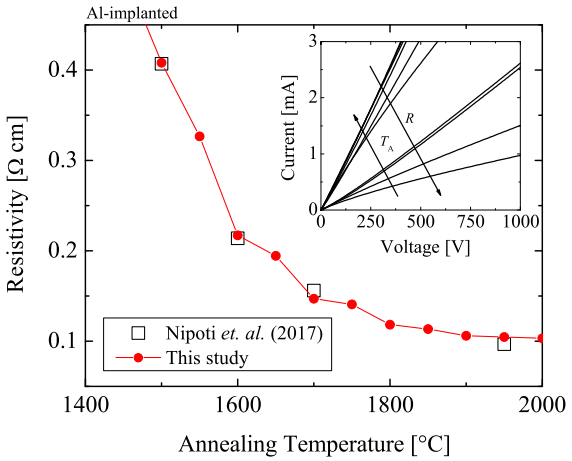


Fig. 7. Resistivity of the Al-implanted SiC as a function of the annealing temperature. Open squares refer to the experimental data from Nipoti *et al.* [25] and the closed symbols refer to the resistivity calculated from the simulations. The inset figure shows simulation results, i.e., current as a function of voltage for samples annealed at various annealing temperatures.

In addition to the verification by comparison with experimental data, we have performed various simulations to predict a minimal required temperature for the full activation of the implants. In the first case of $1 \times 10^{17}$ cm$^{-3}$ Al-implanted SiC, the activation ratio $R_{\text{act}} = 1$ was achieved for the thermal treatments above $T_A = 1700$ °C. In the case of $1 \times 10^{19}$ cm$^{-3}$ B-implanted SiC, $R_{\text{act}} = 1$ was achieved for the annealing steps above $T_A = 1750$ °C. Annealing steps of B-implanted SiC additionally show a high diffusion of B ions over the whole implanted region. However, the diffusion of Al ions was negligible and evident only at the surface. These findings are consistent with the conclusions of Saks *et al.* [17].

To further corroborate the predictability of the model, we have performed device simulations of the processed Al-implanted SiC diodes using the proposed model. The third simulation setup follows the experimental setup of Nipoti *et al.* [25], which consists of an n-type SiC wafer with a compensation concentration of $\approx 3 \times 10^{15}$ cm$^{-3}$, followed by several Al implantations generating a rectangular profile with a mean concentration of $\approx 1 \times 10^{20}$ cm$^{-3}$. The annealing steps were 30 min at $T_A = 1500$ °C, 30 min at $T_A = 1600$ °C, 30 min at $T_A = 1700$ °C, and 1 min at $T_A = 1950$ °C. The mean concentration of this setup exceeds the mean concentrations of the data considered for the model calibration, therefore, these simulations reflect model predictions based on the extrapolation of the model parameters. The resistivity of the variously processed devices, i.e., different annealing temperatures, are shown in Fig. 7. The simulations show excellent agreement with the experimental data, which indicates that the model correctly predicts the devices' properties outside of the calibrated regions as well. The figure in addition confirms the importance of the postimplantation annealing steps, which can be seen by the four-times decrease in resistivity. This further underlines the importance of the proposed activation model, as a 100% activation for high-dose implantation cannot be assumed, but must be accurately predicted, because this critically affects device performance.

## IV. Conclusion

We have investigated the electrical activation of Al and B impurities in SiC and proposed a temperature-dependent empirical model to accurately predict the rate of the dopant activation. The model was fit to preprocessed experimental data to obtain the model parameter $C_{\text{th}}$, which is the key factor to determine the critical saturation region of the electrical activation. The limit of the dopants' saturation effects is annealing temperature-dependent and was found to be in general higher for B-implanted SiC, compared with Al implantation. The temperature dependence has been introduced via Arrhenius functions. The best fits were achieved with $E_a = 2.69$ eV and $E_a = 2.94$ eV for Al and B, respectively. We have calculated predictions of electrical activation ratios for both acceptor-type dopants as a function of total doping concentration and annealing temperature. These results allow to correctly approximate the activation regions and, therefore, further increase the accuracy of device processing simulations, and thus, ultimately, push the SiC technology forward. For the low-dose implantations ($1 \times 10^{15}$ cm$^{-3}$), relatively high activation ratios were achieved for the temperatures below 1200 °C, i.e., a full activation was achieved at $T_A = 1070$ °C for Al-implanted SiC and $T_A = 1010$ °C for B-implanted SiC. In contrast, for the high-dose implantations ($1 \times 10^{20}$ cm$^{-3}$), the full activation of Al impurities was not achieved even at very high temperatures ($T_A > 2200$ °C), but B impurities reached $R_0 = 1$ at $T_A = 2010$ °C. Finally, we have performed simulations to evaluate the model by elaborate comparison with experimental data. The simulations were performed with the Victory Process simulator including the proposed model and parameters. We have reproduced implantation profiles and acceptor concentrations for various annealing steps (i.e., $T_A = 1300$–$1700$ °C) of three individual experimental setups. The results in average show less than 3% variation between the model predictions and experimental findings. Moreover, we have proposed variables of annealing steps to achieve maximal activation of implanted impurities for the investigated SiC devices. Considering time-critical simulations, our model offers a highly attractive balance between accuracy and computational complexity.

## References

[1] T. Kimoto and J. A. Cooper, *Fundamentals of Silicon Carbide Technology: Growth, Characterization, Devices and Applications*. Hoboken, NJ, USA: Wiley, 2014, doi: 10.1002/9781118313534.

[2] W. J. Choyke, H. Matsunami, and G. Pensl, *Silicon Carbide: Recent Major Advances*. Berlin, Germany: Springer, 2013, doi: 978-3-642-18870-1.

[3] Z. Wang *et al.*, "A high temperature silicon carbide MOSFET power module with integrated silicon-on-insulator-based gate drive," *IEEE Trans. Power Electron.*, vol. 30, no. 3, pp. 1432–1445, Mar. 2015, doi: 10.1109/TPEL.2014.2321174.

[4] R. R. Lamichhane *et al.*, "A wide bandgap silicon carbide (SiC) gate driver for high-temperature and high-voltage applications," in *Proc. IEEE 26th Int. Symp. Power Semiconductor Devices IC's (ISPSD)*, Jun. 2014, pp. 414–417, doi: 10.1109/ISPSD.2014.6856064.

[5] B. Whitaker *et al.*, "A high-density, high-efficiency, isolated on-board vehicle battery charger utilizing silicon carbide power devices," *IEEE Trans. Power Electron.*, vol. 29, no. 5, pp. 2606–2617, May 2014, doi: 10.1109/TPEL.2013.2279950.

[6] A. Hallén and M. Linnarsson, "Ion implantation technology for silicon carbide," *Surf. Coatings Technol.*, vol. 306, pp. 190–193, Nov. 2016, doi: 10.1016/j.surfcoat.2016.05.075.

[7] N. Singh, K. Singh, A. Pandey, and D. Kaur, "Improved electrical transport properties in high quality nanocrystalline silicon carbide (nc-SiC) thin films for microelectronic applications," *Mater. Lett.*, vol. 164, pp. 28–31, Feb. 2016, doi: 10.1016/j.matlet.2015.10.107.

[8] V. Šimonka, A. Hössinger, J. Weinbub, and S. Selberherr, "Modeling of electrical activation ratios of phosphorus and nitrogen doped silicon carbide," in *Proc. Int. Conf. Simulation Semiconductor Processes Devices (SISPAD)*, Sep. 2017, pp. 125–128.

[9] R. Nipoti, A. Parisini, G. Sozzi, M. Puzzanghera, A. Parisini, and A. Carnera, "Structural and functional characterizations of $Al^+$ implanted 4H-SiC layers and $Al^+$ implanted 4H-SiC p-n junctions after 1950 °C post implantation annealing," *ECS J. Solid State Sci. Technol.*, vol. 5, no. 10, pp. P621–P626, 2016, doi: 10.1149/2.0211610jss.

[10] A. Parisini and R. Nipoti, "Analysis of the hole transport through valence band states in heavy Al doped 4H-SiC by ion implantation," *J. Appl. Phys.*, vol. 114, no. 24, p. 243703, 2013, doi: 10.1063/1.4852515.

[11] S. G. Sundaresan, M. V. Rao, Y.-L. Tian, M. C. Ridgway, J. A. Schreifels, and J. J. Kopanski, "Ultrahigh-temperature microwave annealing of $Al^+$- and $P^+$-implanted 4*H*-SiC," *J. Appl. Phys.*, vol. 101, no. 7, p. 073708, 2007, doi: 10.1063/1.2717016.

[12] M. Shur, S. L. Rumyantsev, and M. E. Levinshteĭn, *SiC Materials and Devices*, vol. 1. Singapore: World Scientific, 2006, doi: 10.1142/9789812773371.

[13] P. Fedeli *et al.*, "1950 °C post implantation annealing of $Al^+$ implanted 4H-SiC: Relevance of the annealing time," *ECS J. Solid State Sci. Technol.*, vol. 5, no. 9, pp. P534–P539, 2016, doi: 10.1149/2.0361609jss.

[14] N. Saks, A. Suvorov, and D. C. Capell, "High temperature high-dose implantation of aluminum in 4H-SiC," *Appl. Phys. Lett.*, vol. 84, no. 25, pp. 5195–5197, 2004, doi: 10.1063/1.1764934.

[15] *Silvaco's Victory Process Simulator*. Accessed: May 4, 2017. [Online]. Available: http://www.silvaco.com/products/tcad/

[16] J. Weisse *et al.*, "Analysis of compensation effects in aluminum-implanted 4H-SiC devices," in *Proc. Int. Conf. Silicon Carbide Rel. Mater. (ICSCRM)*, to be published.

[17] N. S. Saks, A. K. Agarwal, S.-H. Ryu, and J. W. Palmour, "Low-dose aluminum and boron implants in 4H and 6H silicon carbide," *J. Appl. Phys.*, vol. 90, no. 6, pp. 2796–2805, 2001, doi: 10.1063/1.1392958.

[18] T. Kimoto, O. Takemura, H. Matsunami, T. Nakata, and M. Inoue, "$Al^+$ and $B^+$ implantations into 6H-SiC epilayers and application to PN junction diodes," *J. Electron. Mater.*, vol. 27, no. 4, pp. 358–364, 1998, doi: 10.1007/s11664-998-0415-6.

[19] T. Troffer *et al.*, "Doping of SiC by implantation of boron and aluminum," *Phys. Status Solidi. A*, vol. 162, no. 1, pp. 277–298, Jul. 1997, doi: 10.1002/1521-396X(199707)162:1.

[20] T. Tsirimpis, M. Krieger, H. B. Weber, and G. Pensl, "Electrical activation of $B^+$-ions Implanted into 4H-SiC," *Mater. Sci. Forum*, vols. 645–648, pp. 697–700, Apr. 2010, doi: 10.4028/www.scientific.net/MSF.645-648.697.

[21] M. A. Capano, J. A. Cooper, Jr., M. Melloch, A. Saxler, and W. Mitchel, "Ionization energies and electron mobilities in phosphorus- and nitrogen-implanted 4H-silicon carbide," *J. Appl. Phys.*, vol. 87, no. 12, pp. 8773–8777, 2000, doi: 10.1063/1.373609.

[22] C.-M. Zetterling, *Process Technology for Silicon Carbide Devices*, vol. 2. Stevenage, U.K.: IET, 2002, doi: 10.1049/PBEP002E.

[23] V. Šimonka, A. Hössinger, J. Weinbub, and S. Selberherr, "Modeling and simulation of electrical activation of acceptor-type dopants in silicon carbide," in *Proc. Int. Conf. Silicon Carbide Rel. Mater. (ICSCRM)*, to be published.

[24] A. F. Hayes, *Introduction to Mediation, Moderation, and Conditional Process Analysis: A Regression-Based Approach*. New York, NY, USA: Guilford Press, 2013.

[25] R. Nipoti, A. Carnera, G. Alfieri, and L. Kranz, "About the electrical activation of $1 \times 10^{20}$ $cm^{-3}$ ion implanted Al in 4H-SiC at annealing temperatures in the range 1500–1950 °C," in *Proc. Int. Conf. Silicon Carbide Rel. Mater. (ICSCRM)*, to be published.


**Vito Šimonka** received the Mag. Fiz. (UN) degree (*magna cum laude*) from the University of Maribor, Maribor, Slovenia, in 2015. He is currently pursuing the Ph.D. degree in the area of process TCAD with the Institute for Microelectronics, TU Wien, Vienna, Austria.

Mr. Šimonka received the Rectors Award from the University of Maribor in 2017.

**Andreas Hössinger** is currently the Engineering Manager for process simulation within the TCAD Division, Silvaco Europe Ltd., Cambridge, U.K., who is a leading provider of simulation software for the microelectronics industry. He has co-authored over 40 papers in journals and conferences.

**Josef Weinbub** (M'13) currently holds a senior scientist position with TU Wien, Vienna, Austria, where he leads the Christian Doppler Laboratory for High Performance TCAD. He co-edited six volumes and published 19 articles, 10 book contributions, and 63 conference papers.

**Siegfried Selberherr** (M'79–SM'84–F'93) is currently the Chair Professor with the Institute for Microelectronics, TU Wien, Vienna, Austria. He has authored over 350 papers in journals and books and with his research teams achieved over 1000 articles in conference proceedings.